On the modal behaviour of ultralight composite sandwich automotive panels

On the modal behaviour of ultralight composite sandwich automotive panels

Ana Pavlović, Davide Sintoni, Giangiacomo Minak, Cristiano Fragassa *

Department of Industrial Engineering, Alma Mater Studiorum - Università di Bologna, via Fontanelle 40, 47121 Forlì, Italy

A B S T R A C T

The effects of vibrations in vehicles range from simple noise and reduced comfort, to decreased performance, from wear and material fatigue to irreversible failures and danger. A study of the dynamic behaviour of reinforced composite panels is here presented, applied to the construction of an ultralight photovoltaic roof in the case of a solar sport car. This is an extreme race prototype where design and materials solutions, as high strength carbon fiber reinforced polymers and sandwich-structured composites, were addressed to optimize the stiffness-to-weight ratio. A modal analysis was performed considering materials anisotropies by a layered-shell finite element model and through-the-thickness integration points with the scope to discretize the multi-layered sandwich structure. Additional aspects, as gravity force and external constrains, were also included. Experimental evidences were used for validating the numerical model and underscored an outstanding accuracy. The same design procedure was finally applied to change the preexisting structural solution achieving an optimized roof that was manufactured, installed and tested.

Keywords:
Vehicle design
Roof panel
Stiffness-to-weight ratio
Carbon fiber reinforced polymers
Sandwich-structured composites
Modal analysis
Resonance frequency
Layered-shell

1. Introduction

The use of composite laminates and sandwich panels in automotive, mainly for car frames, is a very effective method to limit the weight while improving the mechanical properties [1]. Due to this, the diffusion of such a type of structures is gradually increasing, especially in motorsport applications [2]. In [3], for instance, a design optimization with the scope to reach the minimum weight of sandwich structures under a combination of torsion and bending loads is proposed. Moreover, in [4], the crashworthy properties of different composite sandwiches are compared as collapsing structures.

At the same time, the determination of an optimal design in the case of composite structures can represent a rather complicated task, since it does not only depend on the inherent complexity introduced by the adoption of composite materials with their own anisotropic properties, but also on the possible complication due to the components' geometry. For instance, in [5] the Ansys Finite Elements (FE) code was used on composites structures to investigate the effect of a frontal impact in the case of a F1 racing car.

The abovementioned studies mainly refer to the use of composite laminates and sandwiches in structural lightening, impact resistance and crashworthiness. However, other investigations also consider additional functions, associated to the dynamic behaviour of composite laminates and sandwiches. For instance, [6–8] deal with dynamic phenomena, transmission of dynamic forces, free forced and damping vibrations, frequencies, damping properties in sandwich composite structures. They also include case studies related to transport and automotive applications.

Actually, almost all structures vibrate creating immediate annoyances, as displacements or noise, and long-term criticalities, as fatigue failure, fretting or wear.

Focusing on the dynamic behaviour of vehicles, the reduction of structural vibrations, which can be caused by engine, wheels, chassis or airflow [9], surely represents a fundamental action in their design permitting to improve smoothness and comfortability in riding [10]. Besides, the same vibrations can also affect the vehicle performance [11] and, even more relevant, the long-term health of passengers [12], to the point of involving structural and personal safety as a whole [13].

To optimize the vibratory behaviour of composite structures, the numerical approach, based on finite elements, is widely utilized, especially in the presence of geometrically complex designs.

In [14] a significant overview about the use of the Finite Element Method (FEM) on composites is reported taking in considerations vibrational problems and dynamic response respect to different materials and applications. The attractiveness of this topic is also reflected in numerous works that aimed at development of efficient and robust finite elements for modeling composite structures, ranging from equiv-

* Corresponding author.
E-mail addresses: ana.pavlovic@unibo.it (A. Pavlović), davide.sintoni@studio.unibo.it (D. Sintoni), giangiacomo.minak@unibo.it (G. Minak), cristiano.fragassa@unibo.it (C. Fragassa).

alent single layer shell elements [15–17], via layer-wise elements [18,19] and up to solid-shell finite elements [20,21]. It also emerges that the numerical modal analysis is preferred as a primary methodological approach for describing, understanding, and modeling structural behaviour in the case of sandwich-structured composites.

The modal behaviour depends on how the structures are made in terms of mass distribution and stiffness. However, modal analysis assumes that the dynamic behaviour of a complex structure, consisting of many degrees of freedom, can be adequately represented through a linear combination of systems, each one characterized by a single degree of freedom [22]. Then, a FEM analysis technique permits to determine these degrees of freedom, even including the presence and the effect of complex geometries or materials [23].

In [24] a parametric study of the influence of the aspect ratio and fiber orientation on the dynamic properties of a fiber-reinforced plate was investigated by FEM. Similarly, the dynamic behaviour of complex structures was also analyzed, such as smart composite beams [25] or composite floors slabs with profiled steel decks [26]. Among other works of particular interest, in [27], the effects of inhomogeneities (delamination damages in the case) on the natural frequencies of a beam was studied, comparing theoretical, numerical and experimental results, and demonstrating even more closely the intimate connection between microstructural and overall properties of the system.

Some studies exploited either shell [28] or solid finite elements [29] to perform a modal analysis of sandwich structures with, respectively, an aluminium honeycomb core and recyclable foam cores. In [30], a modal analysis of a sandwich plate with a central rectangular cutout was performed, highlighting the relations between the natural frequencies and the size of the cutout. Alternatively, a modal mixed numerical-experimental identification procedure for the determination of the elastic and damping properties in the case of sandwich laminates was proposed in [31] where parameters were modified up to a minimum global error between numerical and experimental values.

Among other valuable outcomes emerged regarding the composite sandwiches and dynamics, [32] demonstrated that changes in ply orientation, plate geometry and temperature can affect the dynamic response of FRP sandwich plates with a PVC foam core.

On the other side, [33] studied how the PVC foam core can alter the dynamic response of sandwich materials: an increase in the foam core shear modulus was found to reduce vibrational phenomena. Furthermore, [34] successfully optimized a sandwich structure with a viscoelastic core, maximizing the damping by modifying the layers thicknesses and ply orientations.

The numerical modal analysis of large and complex composite structure was shown in several studies such as a fast patrol boat [35], a wind turbine blade [36] and a chassis frame [37].

An automotive roof, as here mentioned, should be carefully designed considering both its static and dynamic behaviour, and for the scope FEM tools can be a valid support permitting to quickly investigate the effect of design parameters. In [38], for instance, the material choice was optimized by using a FEM model in static and dynamic conditions with a significant reduction in mass of the composite roof. In [39], a similar analysis allowed to optimize the thickness and the lay-up angle of a CFRP laminate, improving bending stiffness instead of weight. FE models have also been used for the topological or material optimization of other automotive components, including the hood, the rear bench and the chassis [40], the floor [41] or the drive shaft [42]. Finally, in [43], the numerical modal analysis was carried out including damping effects with results compared with experiments.

An interesting alternative to the traditional use of laminates, which represent most of the systems analyzed so far, are grid structures or Advanced Grid Stiffened composite structures (AGS) [44], which consist of connected beams. They offer a high damage tolerance and a better dynamic behaviour than conventional sandwich structures. The global and local geometry optimization of a grid structure by using a FEM model is a topic that has been extensively studied in literature, mainly regarding buckling loads [45–47][48,49]In general, FE models offer several advantages over analytical ones, which are acceptable only for initial studies, but it is difficult to fully automatize the process because of the complexities of grid patterns. A refined analytical method, which can be incorporated with existing FEM techniques to obtain a better accuracy, is developed in [50].

2. Aims and scopes

In this paper a reconfigurable photovoltaic roof for a solar vehicle, consisting of a large composite sandwich structure with a quadridirectional grid pattern, is designed by means of an enhanced FE model, able to accurately represent its dynamic behaviour as experimentally verified. Materials characteristics, physical constrains and pre-stress conditions were also considered in detail.

This research is part of a wider action leading to the design and construction of an exclusive solar competition prototype, characterized by a massive use of ultra-lightweight composite structures [51]. Specifically, it represents an evolution, both at the level of methodological approach and technical outcomes, of a recent study [52] where a grid structure, made in sandwich composite, was detected by a multi-objective optimization as the most appropriate design solution of solar roof. The FE model, as here developed, made possible to improve the numerical accuracy and move toward a very efficient design of the sandwich-structured composite in conditions like reality.

To the authors' knowledge, no other research combined the following peculiarities.

Firstly, the study is focused on a rather complex composite structure, both in terms of size and geometry, especially if considered respect to the final application. In the automotive sector, in fact, it is quite uncommon to deal with elements of similar size (8 square meters) and complexity (double orthogonal grid), used as large covering panel (e.g. the roof), but also designed to allow structural functions (e.g. weight support for solar cells).

Furthermore, it is quite unusual to deal with the dynamics of structures with such a complication in terms of materials and layouts: to the seven layers representing the sandwich composite, five layers were added representing the solar panels. These materials were considered respect to their characteristics (e.g. mechanical properties, anisotropy). Some of them (e.g. monocrystalline silicon) are quite rare to be found as subject of dynamic studies and a special state of the art was necessary.

Adding, a specific numerical model was developed with proper attention to refine apparently secondary aspects (e.g. the difference between nominal and actual thicknesses) that was rewarded by the accuracy in the validation phase. The same model was fully exploited to investigate the behaviour of structures in conditions very close to the reality, however complex (e.g. multiplicity of constrains, loads). Hypotheses on models, constraints, forces were compared and discussed.

Finally, the paper is framed in a research area, i.e. the solar vehicles design, still little explored, where results from other sectors (e.g. traditional vehicles) can be rarely transferred in a simple and direct way.

3. Materials and methods

3.1. Vehicle and its geometry

This study, as said, aimed to optimize the movable roof panels in the case of a solar racing vehicle. It is a 4-passenger solar prototype [51] where recent changes in aerodynamics and main structural parts gave the chance to intervene on the photovoltaic roof. In Fig. 1, where the vehicle is shown before and after the intervention, the main differences stand out. In particular, a general rethinking of the vehicle profile with lowering of the rear part to better accompany the flow lines,

allowed a reduction in the aerodynamic coefficients, as drag coefficient (from 0.145 to 0.102) and lift coefficient (from 0.613 to 0.067). At the same time, the extensive use of fiber reinforced composites made it possible to replace the metal safety structure which a composite one with an overall weight reduction and stiffness improvement.

The change in the overall shape of the vehicle and roof was accompanied by a change in the structure of the panel as well. This panel is fixed to the vehicle frame by connecting elements. Its initial structure consisted of a single sandwich panel lightened by circular holes (Fig. 2a). This design solution, in a recent multipurpose optimization proved to be less performing than supposed [52]. Its one-piece structure, with multiple curvature geometry, would have badly adapted to an increase in size as expected from modifications in the vehicle profile (~5200x1.600 mm). Finally, sandwich laminates may represent non-optimal solutions in terms of thermal insulation and, then, solar panel efficiency [52].

A quadrangular grid was preferred (Fig. 2b), made by composite layered rods, connected between them, in a superior orthogonal grid, reinforced by a lower one. This design solution permitted to obtain better mechanical properties [44], but also to simplify the manufacturing and installation phases. In fact, it allowed an easy subdivision of both panel and roof into two sections, which represents a design expedient able to improve their static and dynamic responses as well as handling. Thanks to a reduction in weight and dimensions, in fact, and also to the proper system of constraints, the two sections of the roof can be moved by the pilot in total autonomy for a better orientation with respect to the sun's rays during the parking phases.

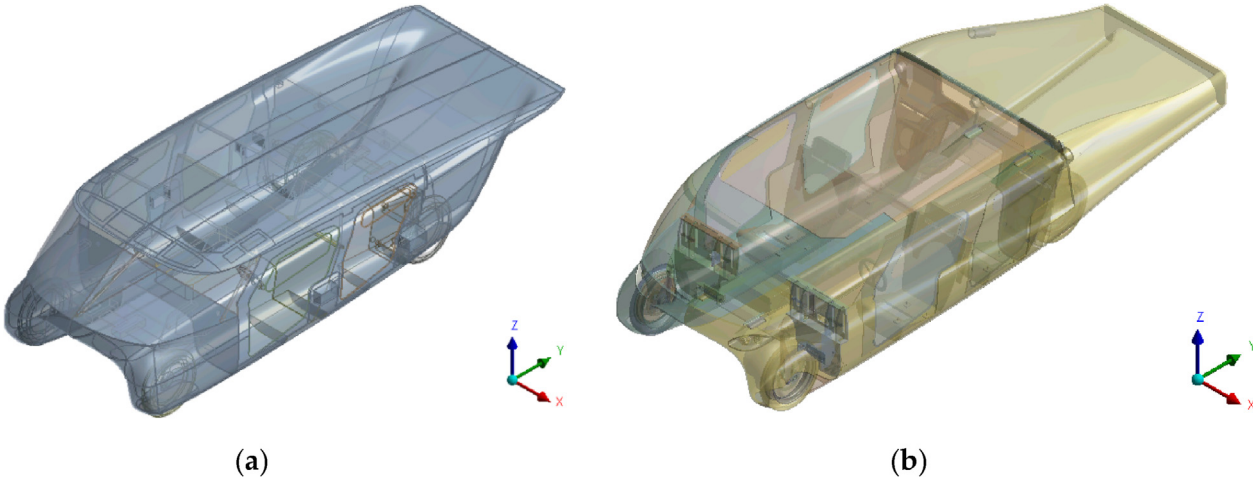

Fig. 1. General layout of multi-occupant solar vehicle: a) before and b) after design changes.

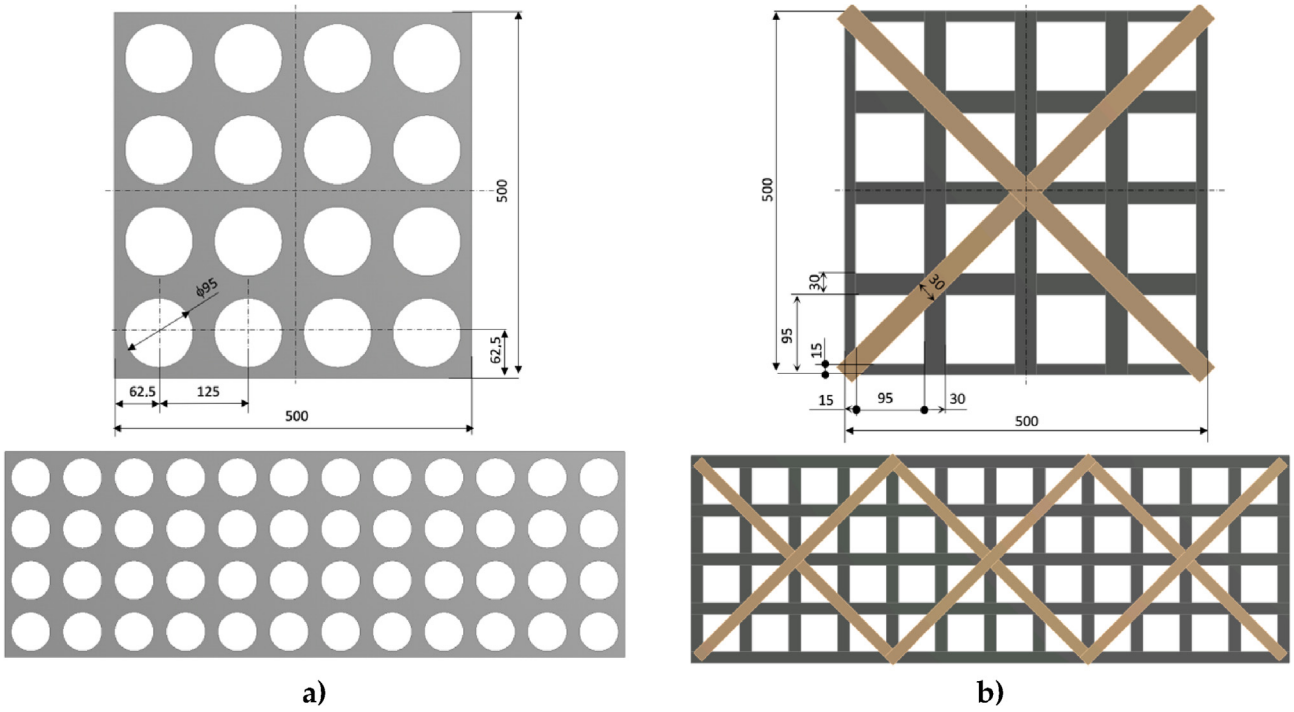

Fig. 2. Structure of the panel: a) before and b) after design changes. The different base elements are reported, together with their special successions in three elements.

3.2. Materials and composite layout

In terms of materials, with the scope to improve mechanical properties and vehicle performance, high strength and stiffness-to-weight ratio materials were adopted wherever possible in the car design. It was also the case of the panel for roof where unidirectional (*UD*) and bidirectional (*BD*) carbon fiber reinforced plastic (CFRP) plies were layered in the form of sandwich structured laminates.

Specifically, *UD* and *BD* CFRP pre-impregnated fabrics (*prepregs*) with, respectively, 0.15 mm and 0.30 mm thicknesses, were used, together with a Polyvinyl chloride (PVC) foam, 4.0 mm of thicknesses, as sandwich core. The 5.20 mm layout consisted of 7 layers, as detailed in Table 1: an outermost BD fabric with fibers are 0°/90°, two UD fabrics at 0°, the core and symmetrical layout respect to this core.

High Tensile Strength (HTS) carbon fibers, with a tensile modulus of 294 GPa and tensile strength up to 6370 MPa of fibers, were chosen. Manufactured by *Toray Composite Materials*, these advanced fibers are largely used in composite structures for automotive when weight reduction is required thanks to their mechanical properties. The UD (namely *T1000*) exhibits, with respect to the fibers' direction, over 120 GPa Elastic Modulus and 2200 MPa Tensile Stress Limit with 1490 Kg/m^3 density. The BD (namely *T800*), with similar density, exhibits in two directions over 60 GPa Elastic Modulus and 800 MPa Tensile Stress Limit. Main properties for these materials are reported in Table 2.

It is important to highlight that in Table 1 the nominal values of the thickness of the pre-preg fabrics as purchased and used to achieve the layering (through manual lamination on an open mold) are shown. However, the manufacturing process in autoclave, including the cure with temperatures around 120 °C and pressures of 2 bars, leads to a decrease in the final thicknesses, estimated at around 10% for the laminates and 15% for the core. The correction was made by an appropriate redefinition of the thicknesses in the FE model so that the materials mass and stiffness referred to a more appropriate geometry.

3.3. Structural dynamic and modal analysis in brief

In general, a dynamic problem can be analyzed with respect to different domains:

- physical domain: complex geometric deformation is represented by a set of independent and simpler deformation models (modal forms) sometimes referable to mathematical formulations.
- time domain: the vibrational response is represented in the form of a signal over time that can be traced back to a set of sinusoids, that tend to fade in the presence of damping phenomena.
- frequency domain: the analysis of the signal over time provides a spectrum containing a series of peaks, then represented by a set of response spectra with a single degree of freedom.
- modal domain: the general response of the system is traced back to an overlap of models, each of which is represented by a mode shape (representing the motion of each points of the structure) and by a modal frequency.

Focusing on this last approach, frequency, mode shape and, eventually, modal damping give a complete representation of the intrinsic dynamic characteristics of the system during vibration. Also, they are constant, related to the structure properties, and FE can support their quick determination.

The modal analysis is the process of determining these modal parameters respect to every mode (in the frequency range of interest) with the goal to use such parameters to build a modal model of the response. This is possible under the two hypotheses that each forced dynamic deformation of a structure can be represented as a weighted sum of its modal forms and that each mode can be represented by a single degree of freedom model.

3.4. Eigenvalues, eigenvectors and normalization

It is also noteworthy how most vibrational problems are related to the resonance phenomenon: in fact, with an excitation of the structure at the resonance frequency, a very small intensity force is enough to induce an oscillation with very high amplitude.

The problem can be traced back to a homogeneous linear system whose non-trivial solution is represented by values, the eigenvalues, which correspond to the deformed ones, the eigenvectors. These eigenvectors have, among their important characteristics, that of being linearly independent vectors, i.e. cannot obtain an eigenvector as a linear combination of the other eigenvectors. Consequently, thanks to this property of orthogonality, they constitute a basis for a vector space (i.e. the modal space). In other terms, the calculation of eigenvectors and eigenvalues as a solution of modal analysis allows the definition of the modes in which it is possible to break down the overall behaviour of the structure into its linear components, and of the natural frequencies against which the structure reacts by entering into resonance.

Despite the link between deformations and eigenvectors, the latter only represent the general shape of the deformed structure, not the actual values of deformation. During the modal analysis, in fact, it is necessary to use a criterion for the normalization of the vector before solving the system.

Thus, modal results (e.g. deformations and elastic deformation energy) are to be considered in relative terms: the amplitude of modal displacements from the eigenvector normalization criterion used. Normalization introduces an arbitrary scale factor on the whole deformed modal shape.

Two normalization criteria are commonly adopted: 1) with respect to the mass of the system or 2) to impose the maximum amplitude equal to the unit. In Ansys Workbench, for instance, the default

Table 1
Sandwich layout.

Layer	Material	Thickness	Orientation
1	BD	0.30 mm	0°/90°
2	UD	0.15 mm	0°
3	UD	0.15 mm	0°
4	PVC	4.00 mm	–
5	UD	0.15 mm	0°
6	UD	0.15 mm	0°
7	BD	0.30 mm	0°/90°

Table 2
Characteristics and properties of materials used for the composite sandwich panel.

Property	Unit	T1000	T800	PVC
Type	–	Unidirectional	Twill	Foam
Density	Kg/m^3	1490	1420	100
Young's Modulus [1]	MPa	121000, 8600, 8600	61340, 61340, 6900	125
Poisson's Ratio[2]	–	0.27, 0.40, 0.27	0.04, 0.30, 0.30	0.40
Shear Modulus[2]	MPa	4700, 3100, 4700	19500, 2700, 2700	44

[1] (X, Y, Z).
[2] (XY, YZ, XZ) directions.

criterion is a normalization with respect to the mass matrix which makes it also complex to compare different geometries in terms of absolute values of deformations and energies. With the scope, it should be considered the Modal Assurance Criterion (MAC), an indicator which gives the degree of consistency between two modal vectors and thus permits to compare mode shapes obtained with different methods [53]. Instead, it remains possible to compare the different solutions in terms of mode shape and eigenvalues, as done in the present case.

3.5. Discretisation model

The numerical modal analyses were performed using Ansys Workbench Ver. 19 software and SHELL181 elements. This two-dimensional (shell) element, characterized by 4 nodes and 6 degrees of freedom (DoF) in each node, was preferred due to its fitness in the case of large rotations or large deformations, but also considering others' positive experiences in modelling composite laminates and sandwiches (as in [54,55]).

In addition, with the scope to take in consideration the stratification the so-called layered shell method was applied. It consists in a discretization, common in the structural analysis of composite laminates, based on shell FEs (SHELL181 in the case) along the surface and Integration Points (IPs) through the thickness. This method overcomes the need to operate with solid (3D) elements with significant savings in terms of computing effort and an accuracy often adequate to the needs [56,57].

In dynamic analyzes it is customary to refer to the discretization techniques already proven valid for structural analyzes. Consequently, in addition to the selection of the layered shell method, it was also chosen to limit the IPs to one per each layer.

However, rather than limiting the IPs to 7, equal to the number of sandwich layers, it was decided to adopt another arrangement, already used in structural analyzes by a layered shell method [56]. On such occasions, the problem often arises of finding a way to investigate what happened in terms of out-of-plane phenomena (e.g. delamination) and a possible way is to consider the various layers joined by a thin layer of pure resin. This assumption intends to take into account the fact that during the autoclave cure, adjacent layers of prepreg solidify together, merging each other in terms of resins, without however making possible a physical cross between the fibers.

It follows that the discretization in the thickness was carried out through 13 IPs, since an addition of 6 IPs in relation to the interlaminar zones. Fig. 3 shows the presence of these IPs through the 5.2 mm sandwich thickness, both in the laminates and in the resin interfaces. The same figure also shows the location of FEs and nodes on surfaces. According to some preliminary tests done for the model calibration, although this finesse in terms of material modeling has a minor effect ($<2\%$), still leads to results more in line with reality, slightly raising the natural frequencies.

4. Results and discussion

4.1. Model validation

A first simulation was performed with the scope to validate the numerical model by experiment. A test specimen was manufactured planarly coupling, side by side, three quadrangular grids (Fig. 2b). During the modal test, the structure was raised and suspended using an elastic wire and two anchoring points placed symmetrically. The dynamic response to the induced stresses was detected through accelerometers by measuring natural frequencies up to 125 Hz (including the first 6 modes for rigid body movements). Mechanical vibration and shock tests were performed in accordance with ISO 7626-5:2019 and, specifically, with Part 2 and Part 5 [58,59]. Additional details on the testing procedure are also available in [52].

The comparison would have to repeat a modal test under *free-free* conditions: no constraints or forces. However, with the aim of improving the accuracy of the numerical model, it was decided to take into account all the identified conditions that could have influenced the results. In particular, as regards the validation phase, the effect of gravity was introduced in the study. For the purpose, the modal analysis was anticipated by a static analysis that allowed to demonstrate a negligible deformation caused by the gravity force, lower than 0.02% (more pronounced effects emerged in next simulations. Both aspects, *free-free* condition and gravity effects on modal analysis, will be explored in the discussion of results).

The numerical modal analysis was limited to the evaluation of the first 20 eigenvalues where the first 7 were compared with the system natural frequencies as detected from experiments. Fig. 4 permits an initial visual evaluation of results showing, side by side, the equivalence between mode shapes. No difference seems to emerge with simulations able to correctly reconstruct the deformation trend. Table 3 permits a numerical assessment providing results in terms of natural frequencies. It is immediately evident the great accuracy of the model with rather negligible errors (apart in one case, the 6th frequencies). Furthermore, the accuracy in predicting the first frequency, which is usually the most interesting since the connection with the minimum level of energy resonances start to emerge from, is very high. Finally, a minor but quite common underestimation of natural frequencies seems also evident which suggests a refining in model discretization can be even possible.

Above the 7th at 124.69 Hz, unfortunately, no measure was available since the detection was limited to approx. 125 Hz. Experimental information should be of special interest in this range considering an

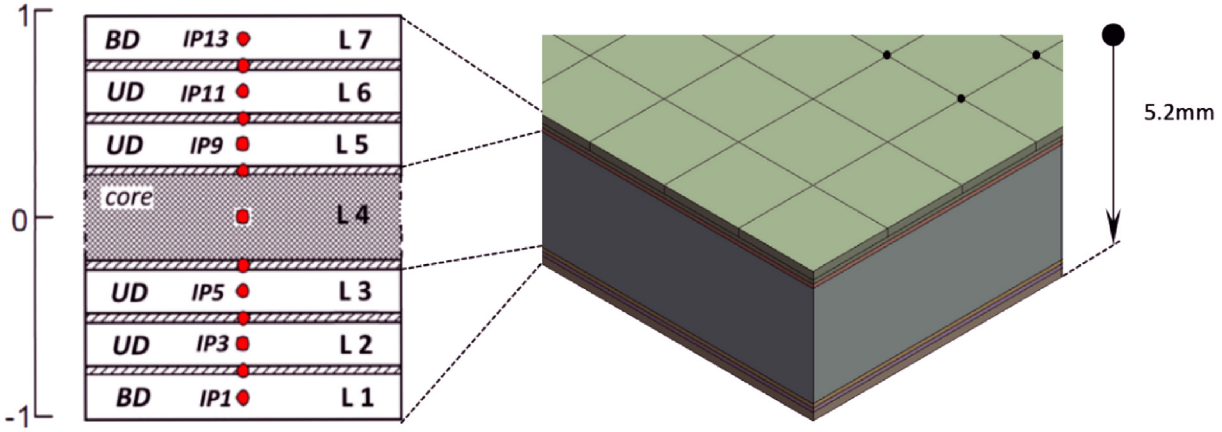

Fig. 3. Through-the-thickness IPs for a 7-layers laminate with extra IPs at interface.

anomalous closeness between some natural frequencies: the 8th at 126.69, very closed to 7th or 9th and 10th at, respectively, 142.32, 142.48 Hz. An analysis, based on frequencies so close each other, could represent a valid test bench to new hypotheses and model refining.

4.2. About the validation

4.2.1. Free-Free modal analysis

The characteristic equation of a structure allows a solution even without introducing constraints into the system. Natural frequencies also exist, in fact, for a body that is suspended in the air, without restrictions (namely, a free-free system). When performing a modal calculation in these conditions, 6 eigenvectors with very low frequency, close to 0 Hz, emerge. These eigenvectors represent the forms of rigid body movements, that is, the roto-translation oscillations that the system performs in space. After these, at higher values, frequencies emerge that represent the elastic modes. In addition, many of the experiments are usually traced to this free-free situation, as in the case described here, where the structure under test was hung on an elastic support by means of two contact points. However, in order to achieve the greatest accuracy, the numerical model also took into account this difference between free-free and real testing conditions, however minimal. In particular, the system was analyzed considering the constraints actually used (elastic supports) through a first static analysis that affects the results of the modal analysis by providing as input a system with matrix deformed by the load and constraint conditions. Thus, thanks to what is defined as 'pre-stressed modal analysis', it was possible to eliminate a possible source of bias (i.e. constraints).

4.2.2. Gravity

Even the effects of gravity and dead weights shall be considered. The static deflection, in fact, modifies the stiffness of the structure, causing a difference in the dynamic properties if compared to the nominal ones [60]. In [61], for instance, a modal analysis was performed on a prestressed shell structure. After applied a pressure load on the surface, the results showed that preloading did not affect mode shapes but impacted on the natural frequencies. Some studies considered preloading conditions during dynamic analyses as [62] that applied the dead weight of the chassis to a truck frame or [63] that a gait frequency structure with a gravitational load was examined. These evidences led to the inclusion of gravity force among the effects to be monitored.

Operationally, the effect of self-weight on the modal response of the structure can be taken into account in two alternative ways: a) in the pre-stress analysis by applying a load vector that represents the gravity force for intensity and direction; b) in the modal analysis by activating the standard earth gravity command. In both cases, the materials densities must be defined among the properties. In the specific case, both procedures were used verifying a full correspondence in the numerical outputs.

4.3. Model application

The same numerical model and approach were used on the solar roof as a whole. Structural modules, based on quadridirectional grids, were merged to rebuild the real 3D geometry of the roof. Design and manufacturing aspects (e.g. edges, shrinkages, partitions) were also considered. The final sandwich structure is shown in Fig. 5 where it

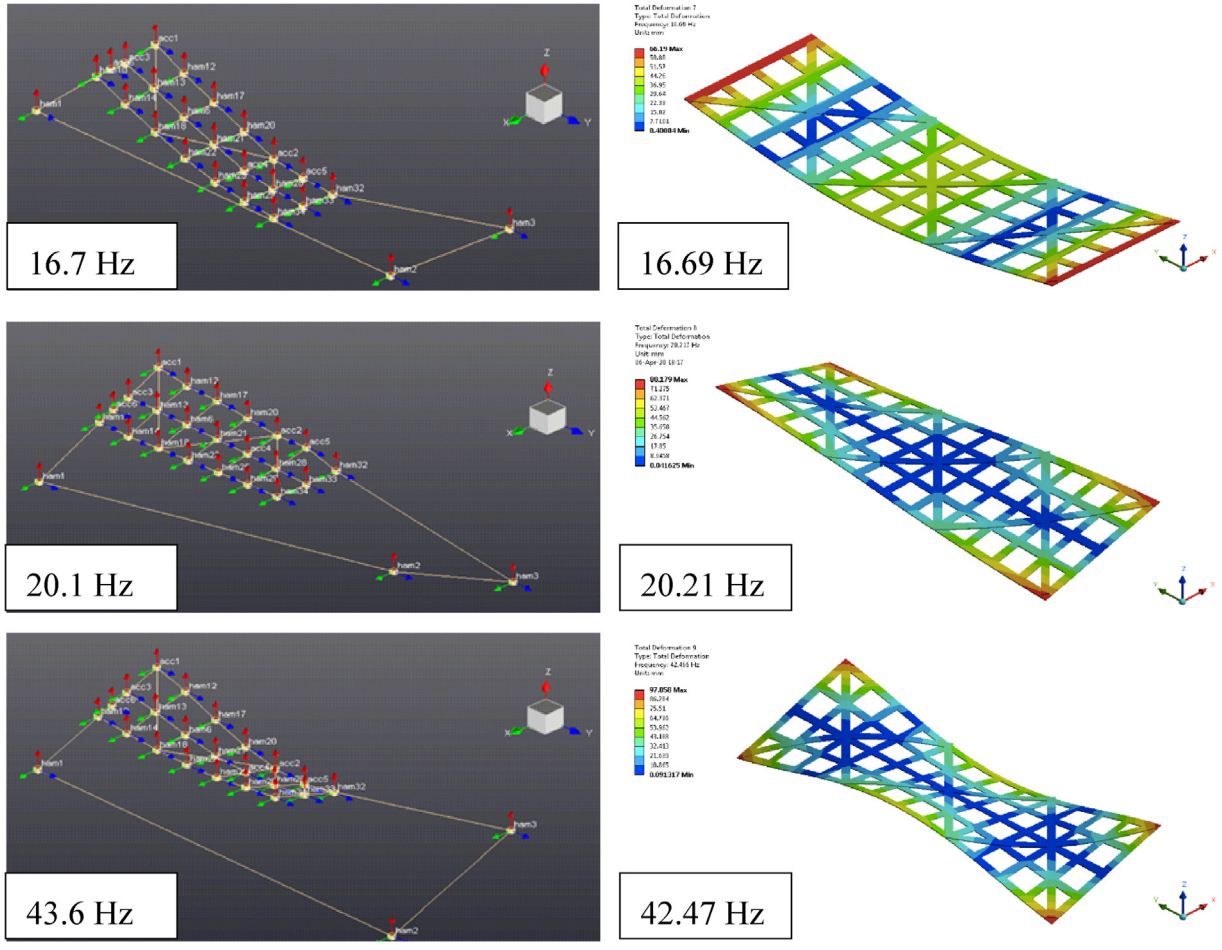

Fig. 4. Results for modal analysis: a) experiment and b) simulation.

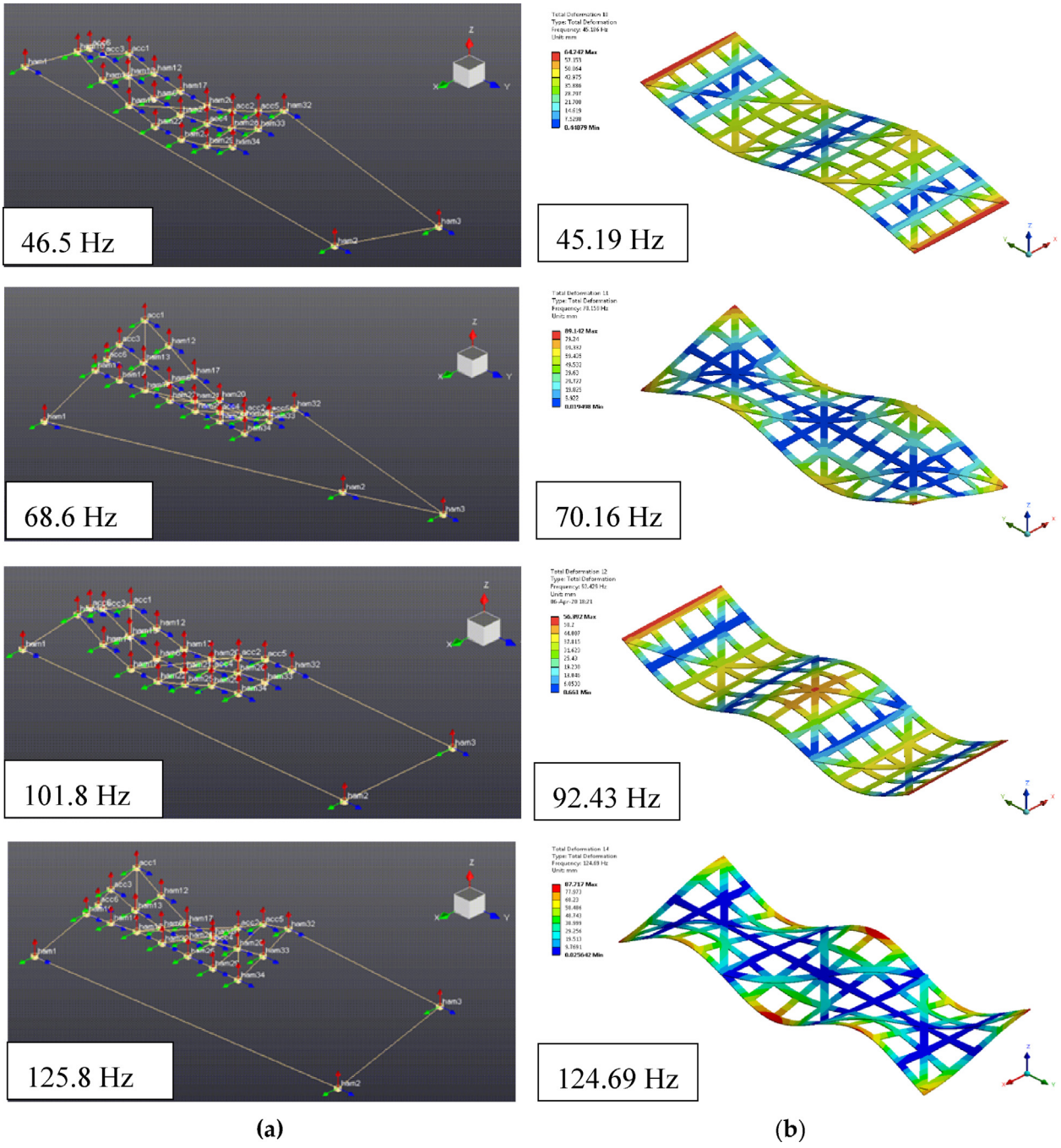

Fig. 4 (*continued*)

Table 3
Comparing the results from modal analysis in terms of natural frequencies.

Mode	Natural Frequency (Hz)		Error (%)
	Measure	Simulation	
I	16.7	16.69	−0.06
II	20.1	20.21	0.55
III	42.6	42.47	−0.31
IV	46.5	45.19	−2.82
V	68.6	70.16	2.27
VI	101.8	92.43	−9.20%
VII	125.8	124.69	−0.88%
		average	−1.49%

is also evident the subdivision in front and rear parts. Table 3 reports the overall dimensions of these composite structures.

In Fig. 5, the material layout is also reported. Nothing was changed respect to the previous case.

Thus, material model remained the same. However, a difference emerges regarding constraints.

As first, grids are not in free-free conditions but positioned on a rigid frame (i.e. the vehicle safety cage and main structures that can be assumed for the present investigation as a fixed basement). In addition, two hinges on the left side permitting the roof rotation around the y-axis and six joints on the opposite side fixing it were considered. This combination of constraints allows, with the vehicle parked, to unhook and rotate the solar roof in the direction of the sun thus

optimizing the efficiency of the photovoltaic panel in capturing energy during competition.

The situation can be conventionally represented and simplified as a *simple* support on the entire edge, two *roller* and six *fixed* supports in specific zones (as shown in Fig. 5).

These constrains were included in the modal analysis passing by the pre-stressed analysis.

Furthermore, unlike the system used for validation, in this case the composite structure supports the solar cells which affect the dynamic behaviour both in terms of weight and stiffness.

The photovoltaic cells, in monocrystalline silicon, *E60 bin Me1* by SunPower®, were directly laminated on the sandwich panels (by Solbian®). A 1.5 mm layout was used consisting of two layers of thermoplastic polyolefin (TPO) as encapsulating films, one layer in Ethylene tetrafluoroethylene (ETFE) as protecting front-sheet and one layer in Polyethylene terephthalate (PET) as back-sheet.

The new condition of mass and stiffness was considered involving the mechanical properties of missing materials (Table 4) and applying in accordance with the layered shell model. Specifically, the CAD model was changed in the way to provide new design elements. Each of these elements exactly represents a photovoltaic modulus in terms of dimensions shape and positioning on the roof. Then, they are characterized by layout and material properties, before implementing the modal analysis.

Material properties derive from [64–73]. In the case of variability, an average value was chosen (e.g. 158.5 GPa for Young's Modulus of monocrystalline silicon that ranges between 130 and 187 GPa).

4.4. Modal analysis

Three different numerical analysis were performed, one per each of the following systems:

a. quadrangular grids in free-free conditions (namely '*free-free*')
b. quadrangular grids with constrains ('*constrained*')
c. quadrangular grids and solar cells with constrains and weight ('*pre-loaded*')

Replicating the study under conditions of growing complexity allowed to investigate the effects on the roof modal behaviour of each aspect of interest. In particular, while the 1st and 2nd investigations could be performed by a modal analysis, respectively free or constrained, in the 3rd case it was necessary to carry out a pre-stress analysis. Results are reported in Table 5 in terms of eigenvalues and discussed in the following sections.

4.4.1. Free-Free system

The modal analysis started considering, as said, two quadrangular sandwich grids representing the rear and front portions of the roof. The influence of the solar panel, with its mass and stiffness, was not included at this stage. Grids were analyzed in free-free conditions. i.e. without external forces or constrains. Neglecting rigid body motions (first six natural frequencies), the earliest three frequencies were detected at 10.0, 15.9 and 19.0 Hz for the rear section and 12.4, 21.3 and 27.5 Hz for the front section with mode shapes and displacements shown in Fig. 6. The initial 12 eigenvalues from the numerical solution are reported in Table 5. Although at an initial phase of evaluation, the higher criticality of the rear section (i.e. lower eigenvalues) is already evident. It intrinsically occurs even in the presence of lower sizes (about −30%) and maybe depends on the specific shape, like a flat plate. without the three-dimensional frame that preserves the front section from instabilities

4.4.2. Constrained system

The modal analysis, then, was performed on the same system, but including external constrains. The two quadrangular sandwich, grids

Table 4
Overall geometrical dimensions for roof sections.

Section	Dimensions [m]	Surface [m^2]	Weight [Kg]
Front	1.681 × 2.344 × 0.116	2.433	5.02
Rear	1.540 × 2.077 × 0.510	1.801	3.72
Total	1.610 × 2.210 × 0.313	4.244	8.74

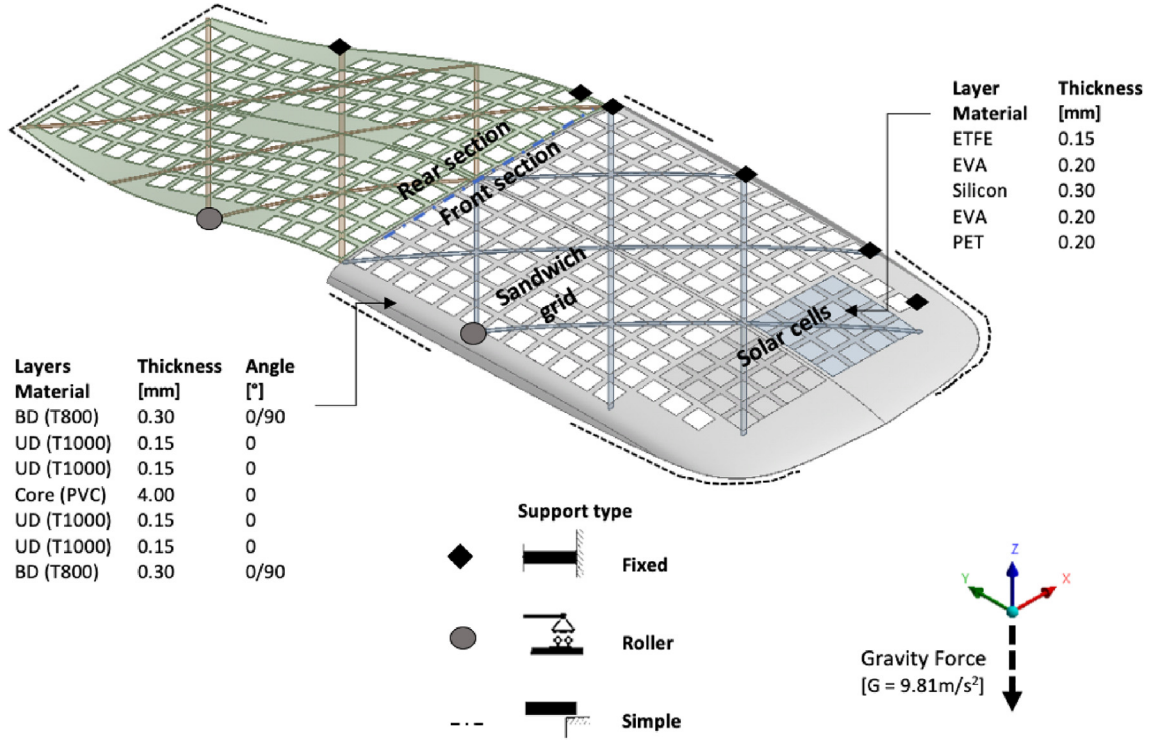

Fig. 5. Vehicle roof with details on main structures, materials, layers, loads and constraints.

Table 5
Characteristics and properties of materials used for the photovoltaic panel.

Property	Unit	Silicon	TPO	ETFE	PET
Density	kg/m^3	2327	850–1820 [66]	1800 [68]	1410 [70]
Young's Modulus	MPa	130–187 000[64]	986–2100 [66]	1500 [69]	1700 [70]
Poisson's Ratio	–	0.20–0.28 [64]	0.49 [67]	0.43–0.45 [69]	0.37–0.44 [71]
Shear Modulus	MPa	51–79 000 [65]	10–175 [67]		27.9–50 [72]

representing the rear and front portions of the roof, and without considering the effect of the solar panel, were investigated. The presence of physical (fixed, roller and simple) constrains was added. Specifically, in accordance with Fig. 5, the rear and front panels were considered as simply supported by a frame able to prevent vertical transactions and to permit rotations. In addition, each panel was constrained by one *roller* and three *fixed* supports (located in precise segments on opposite edges). Since structures completely constrained, no rigid body motion was present and the earliest three frequencies were detected at 9.2, 14.3 and 19.5 Hz for rear section and 13.3, 24.4 and 28.9 Hz for front section with modal shapes as displayed in Fig. 7. The related list of eigenvalues is reported in Table 5.

The effect on the dynamic response on the application of different constraints was also deepened by replicating the modal analysis for each constrain, independently. In short, it was possible to observe that *simply supports* slightly modifies free-body frequencies. This constrain acts by fixing only 1 on 6 degrees of freedom of rigid body so that the first 5 eigenvalues had to be neglected. Comparing not-trivial eigenvalues, differences were minimal, both in terms of frequencies and mode shapes.

On the contrary, the addition of further constraints significantly changed the behaviour of the structure increasing its stiffness. This is evident from the new eigenvalues, as shown in Table 6, limited to the rear section. In particular, the table compares the lowest eigenvalues considering different constrain configurations: free-free, simply support (respect to the vertical axis) and a combination of constrains as described. A further condition was also considered in the assessment (named as 'fully constrained' in the table). It was obtained setting the simply support constrain along the edge able to fix movements (but not rotations) along the three directions. This condition can represent a design limit in term of stiffness of the constraints, when, as is already foreseen, the coupling between the panel and the roof frame are made by means of gaskets.

4.4.3. Pre-loaded system

Since the stress state of a structure under constant static loads, as gravity, may affect its natural frequencies, a linear static analysis was performed considering both sandwich and cells own weight. Thanks to this pre-analysis it was also possible to take into account the solar cells stiffness. A stress stiffness matrix was calculated from this structural analysis and the origin vibration equation was modified including the stress stiffness matrix. The structural analysis kept saved the constrains as previously defined. The related list of eigenvalues is reported in Table 5.

It can be observed how the weight addition for of a well-constrained structure (front part) leads to a general stiffening with a

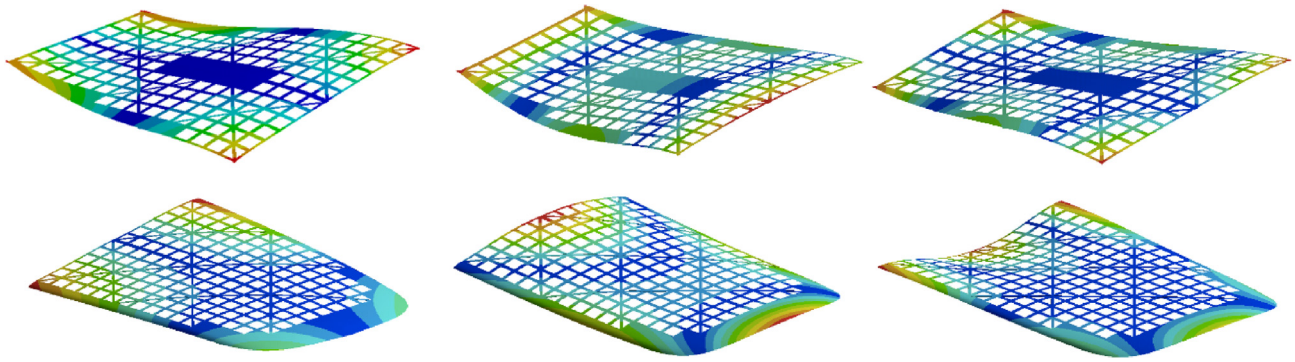

Fig. 6. Earliest mode shapes and displacements for rear and front sections of the sandwich structures (without solar cells) in free-free conditions.

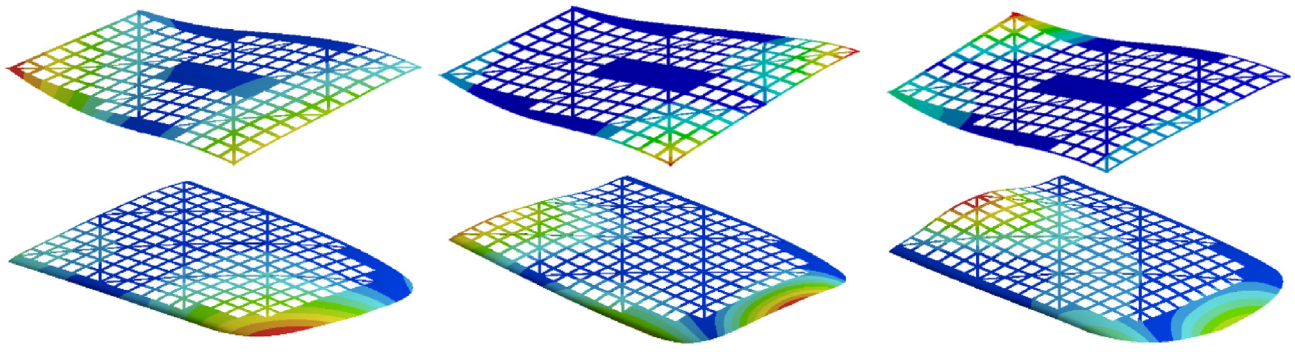

Fig. 7. Earliest mode shapes and displacements for rear and front sections of the sandwich structures (without solar cells) in constrained conditions.

Table 6
List of lowest natural frequencies (eigenvalues), in Hz, from the numerical solution.

	Rear Section			Front Section		
Eigenvalue	Free-Free	Constrained	PreLoaded	Free-Free	Constrained	PreLoaded
1	10.0	9.2	8.7	12.4	13.3	19.5
2	15.9	14.3	13.5	21.3	24.4	25.2
3	19.0	19.5	18.7	27.5	28.9	31.1
4	24.8	26.7	25.4	32.7	31.9	43.5
5	32.8	32.3	31.5	42.3	46.8	44.9
6	34.1	35.3	34.8	46.3	49.3	48.2
7	43.4	47.2	46.2	48.0	55.2	54.7
8	57.1	51.2	50.6	56.6	57.3	60.0
9	57.7	54.9	53.9	61.2	64.0.3	62.4
10	60.9	57.5	57.1	63.9	71.2	71.9
11	61.1	63.6	63.1	68.8	75.9	73.4
12	73.8	67.1	66.8	74.4	77.4	77.8

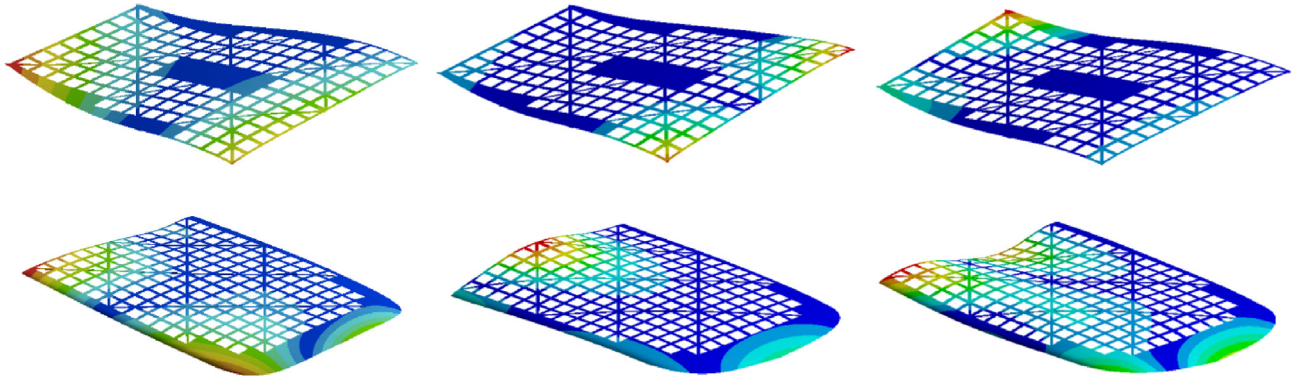

Fig. 8. Earliest mode shapes for rear and front sections of the roof, including presence of solar cells, in loaded (by gravity) and constrained conditions.

progressive raising of the frequencies to the strengthening of the constraint conditions (from 12.4 Hz of the free-free system, through 13.3 Hz for constrained up to 19.5 Hz for preloaded in the case of first eigenvalue). It does not happen the same when the structure is not correctly constrained (as the rear part) where, on the contrary, an increase in the conditions of constraint slightly reduces the natural frequencies (from 10.0, passing by 9.2 to 8.7 Hz).

Finally, the effect of the presence of the solar cells on the sandwich in terms of structure dynamics was also deepened by replicating the modal analysis for different modelling conditions (Fig. 8). For instance. it was investigated what occurred when mass and stiffness of solar cells were considered as uniformly distributed on the composite structure instead of located in specific sections of the roof (as in the real case) finding rather marginal differences. This relevant outcome made it possible to simplify the roof modeling by changes in the composite layout and without including additional CAD elements (visible in Fig. 5).

4.5. Resonances

One of the main scopes of the modal analysis, in brief, is to avoid the risk that natural frequencies of a structure are too close to the

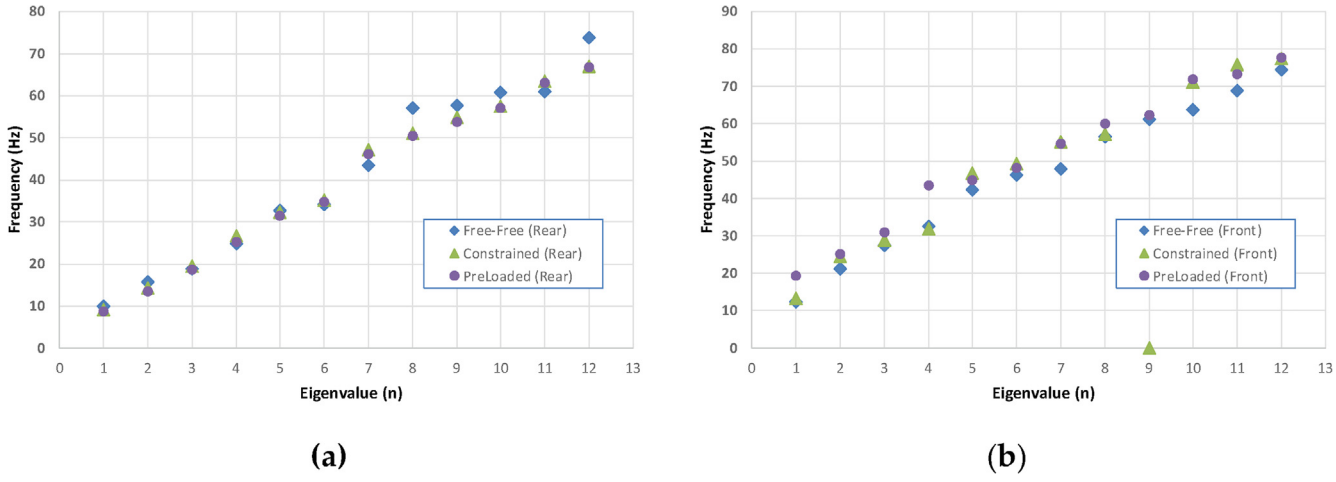

Fig. 9. Comparing resonance frequencies respect to the three different systems under investigation for a) rear and b) front sections.

expected frequencies of external forces since this physical situation could cause resonance phenomena.

No investigation on the topic, specifically focused on solar vehicles, exists while they are almost different in terms of vibrations respect to traditional endothermic vehicles to permit a direct use of available results. However, several studies refer the dynamic response of Electric Vehicles (EVs) which can be taken as a valid point of reference. In [74], for instance, the vibration to which are exposed three commercial EVs during a 100,000 miles life were analyzed, determining EVs are subjected to a resonant peak, related to the dynamics of the powertrain, generally between 7 and 20 Hz, with measured peaks around 11 and 13 Hz. [75] investigated three EVs with different design configurations (in-wheel motor, direct drive, electric motor with reduction and differential gears), distinguishing common resonant peaks slightly under 10 Hz for longitudinal road excitations and slightly above 10 Hz for vertical road excitations. Similar values are also reported in [76].

Another potential source for initiating resonance effects is related to aerodynamic aspects and, in particular, the pressure of microturbulences on surfaces. These phenomena, investigated on other types of vehicles, are more difficult to be generalized starting from literature data because they are highly dependent on the geometries, surface qualities and speeds involved.

Given all this, Fig. 9 summarizes the earliest frequencies as detected by simulations for rear and front sections respect to the three different physical models under investigation. Frequencies below 20 Hz are those to be taken into greater consideration given the greater risk of initiating resonance phenomena.

4.6. Within the numbers

Some of the results already anticipated can be lastly confirmed and new ones added:

- as it was to be expected, the application of constraints causes a general improvement in the structure stiffness with a consequent increase in the natural frequencies; this increase is however offset by the fact that the structures' own weights are applied;
- it follows that, in the specific case under investigations, the structures, under constrains and weights, behave in a way not dissimilar to a free-free condition in terms of eigenvalues;
- nevertheless, the addition of constraint conditions strongly changes the mode shapes creating new situations in terms of criticality;
- the rear is the most critical between the two sections, despite its lower weight, with a natural frequency (~10 Hz) lower than to the typical values of resonance of EVs (~11–13 Hz)
- this situation can be explained by an under-constraint conditions which make the behaviour of the constrained structure rather similar to that one characterizing the free-free structure with an (almost) overlapping between the eigenvalues (< 10% of differences).
- as design solution, it is certainly necessary to provide additional constraints (e.g. gaskets) moving toward the case of 'full-constrained' along the full edge where displacements (but not rotations) are forbitten and eigenvalues increased to ~ 55 Hz;
- these precautions are useful but not strictly necessary for the front part which exhibits higher own frequencies (~30 Hz).

4.7. Participation factors and Effective masses

As said, the value of displacements from modal analysis has not a real physical sense. The same happens for stresses and strains. Nevertheless, to better analyze the results, additional aspects as Participation Factors and Effective Masses (by its factors) should be also considered.

The Participation Factor (PF) measures the amount of mass moving in each direction for each mode. A high value in a direction indicates that the mode will be excited by forces in that direction.

The Effective Mass (EM) provides, similarly, a measure of the energy related to each resonant mode since it represents the amount of system mass participating in the mode. The total amount of EM respect to each mode should be equal total mass of structure.

Therefore, it can be imagined that a mode characterized by larger PF and/or EM can represent a significant contributor to the overall response of the system

As an example of factors' usability, Table 7 and Table 8 respectively report PF (adimensional) and EM (in kg). These values, available as a direct reading from the code output, are here limited to the rear section and to the first 8 resonances (up to ~ 50 Hz) (Table 9).

It can be seen, e. g., that the 4th frequency, at 25.4 Hz, probably represents the most critical one: there is an evident structure participation, both in terms of energy (EM) and in mass (PF), 10 times higher respect to other resonances. Adding, the phenomenon seems to involve two directional (Y and Z) and one rotational (RX) axes. Similarly, the 5th and 7th frequencies (at 31.5 and 46.2 Hz) are to be kept under observation, especially as regards to the Z-axis direction and the X-axis rotation (RX).

Table 7
Natural frequencies (eigenvalues) of the rear section for different constrains (in Hz).

Eigenvalue	Free-Free	Simply	Constrained	Fully Constrained
1	10.0	9.9	9.2	54.9
2	15.9	11.5	14.3	59.1
3	19.0	18.9	19.5	78.1
4	24.8	23.2	26.7	87.7
5	32.8	32.7	32.3	92.8

Table 8
Participation Factor (PF) of the rear section.

	Frequency	Direction			Rotation		
N.	Hz	X	Y	Z	RX	RY	RZ
1	8.7	1.11E−03	1.14E−03	7.39E−03	5.88E + 04	4.28E + 04	−5.38E + 04
2	13.5	2.86E−03	−7.65E−06	−2.64E−03	−1.65E + 04	−1.00E + 04	−5.62E + 04
3	18.7	−8.37E−04	−3.98E−03	−9.90E−03	−2.42E + 04	−9.61E + 04	5.22E + 04
4	25.4	−2.88E−03	−1.11E−02	−3.64E−02	−1.35E + 02	−4.32E + 04	1.22E + 04
5	31.5	4.12E−03	4.42E−03	1.63E−02	6.25E + 04	−6.55E + 04	−1.23E + 04
6	34.8	1.61E−03	−2.18E−03	2.20E−03	1.58E + 04	−3.84E + 04	−5.09E + 04
7	46.2	1.85E−03	−6.94E−03	−1.81E−02	−6.05E + 04	−3.76E + 04	−5.76E + 04
8	50.6	−4.38E−03	−1.58E−03	−7.89E−03	−2.88E + 04	2.26E + 04	1.28E + 04

Table 9
Effective Mass (EM) of the rear section (in kg).

	Frequency	Direction			Rotation		
N.	Hz	X	Y	Z	RX	RY	RZ
1	8.7	1.23E−06	1.29E−06	5.46E−05	3.46E + 03	1.83E + 05	2.89E + 05
2	13.5	8.15E−06	5.85E−11	6.95E−06	2.72E + 05	1.01E + 05	3.16E + 05
3	18.7	7.00E−07	1.58E−05	9.79E−05	5.85E + 05	9.24E + 05	2.72E + 05
4	25.4	8.27E−06	1.23E−04	1.33E−03	1.82E + 04	1.87E + 05	1.50E + 05
5	31.5	1.70E−05	1.95E−05	2.65E−04	3.91E + 03	4.29E + 05	1.51E + 05
6	34.8	2.61E−06	4.74E−06	4.85E−06	2.49E + 05	1.48E + 05	2.59E + 05
7	46.2	3.41E−06	4.81E−05	3.29E−04	3.66E + 03	1.41E + 05	3.32E + 05
8	50.6	1.92E−05	2.51E−06	6.23E−05	8.30E + 05	5.12E + 05	1.63E + 05

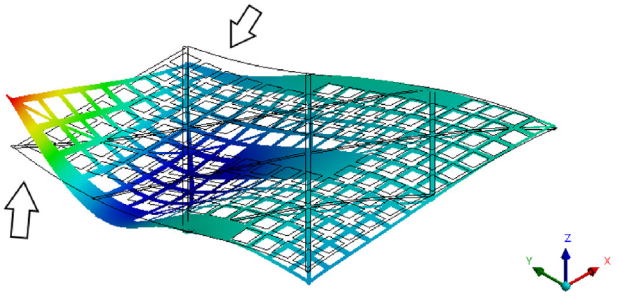

Fig. 10. Displacement respect to the 4th frequency (25.4 Hz).

About more general considerations, it is possible to observe, e.g., how the most critical issues are present with respect to the Z-axis direction (as was to be expected), both in terms of energies and masses. Between them, EM is probably the most critical factor, especially respect to rotations. In this regard, it is also interesting to note the presence of a rather high value for EM (3.46E + 03) at the 1st frequency (8.7 Hz) with respect to the X-axis rotation (RX) which could make necessary to intervene despite all the other values indicating negligible PF and EM in the first 3 frequencies (<25 Hz).

Once the most critical conditions were identified through these factors, both in terms of frequencies and directions and conditions (i.e. energy or mass), it became easier to investigate the phenomena. For instance, Fig. 10 reports the 4th frequency (25.4 Hz) which had

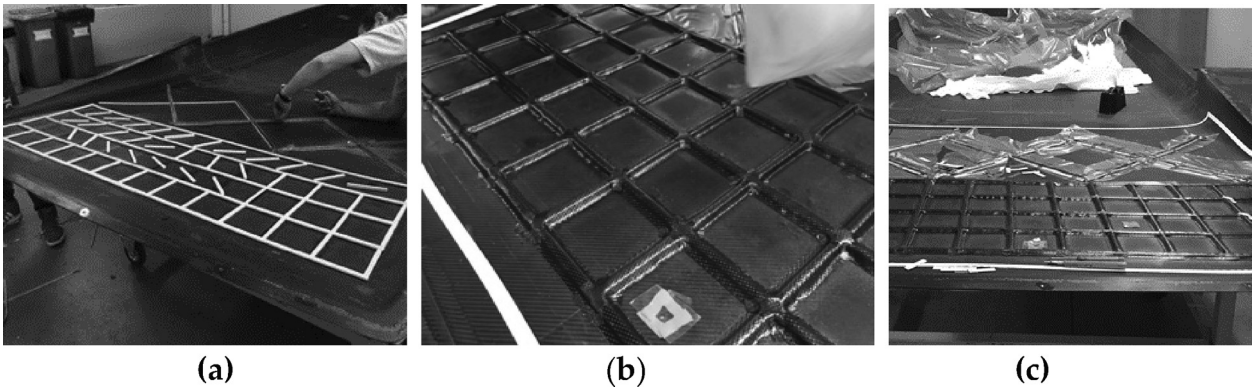

Fig. 11. Three steps in the sandwich panel manufacturing: a) positioning of the first segments necessary to build the grid; b) first orthogonal grid; c) superposition of the two orthogonal grids.

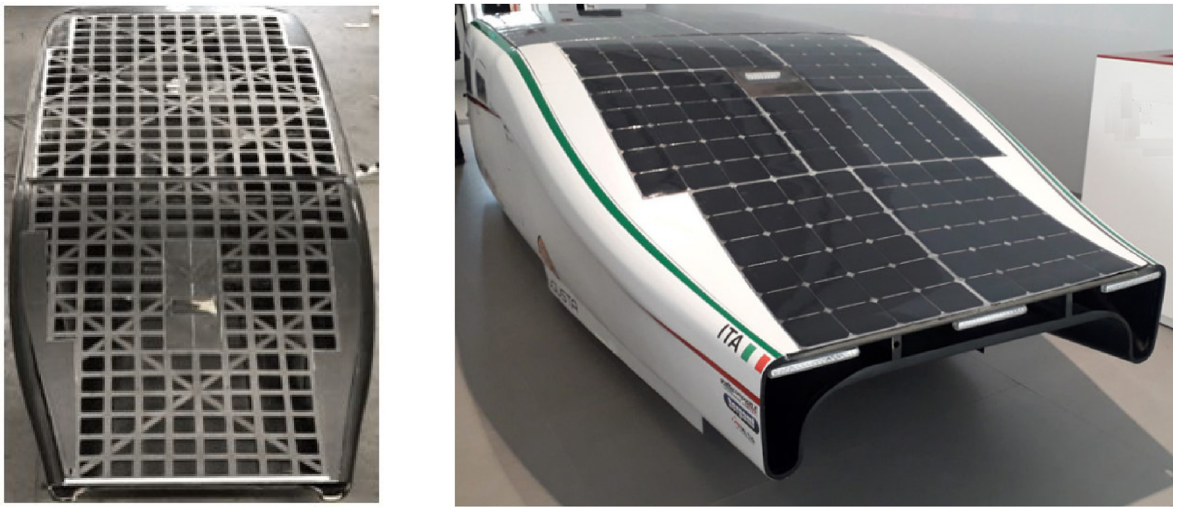

Fig. 12. Final stages of construction of the solar roof: a) the composite sandwich structure is positioned on the vehicle frame; b) the roof is completed with solar panels.

appeared worthy of further study especially respect to Y and Z direction and RX rotation. The image makes clear, e.g., the need to fix the rear corner of the panel differently.

4.8. Manufacturing

Ultimately, it was possible to move on to the phase of solar roof construction. In particular, in Fig. 11 three steps related to the sandwich panel manufacturing are shown while Fig. 12 exhibits the entire sandwich panel on the vehicle frame, before and after installing the photovoltaic cells.

4.9. Overall investigation at a glace

This investigation, in brief, followed these subsequent steps:

1. the modal analysis was chosen as domain and finite elements as tool;
2. a quadrangular grid was designed and used as base element;
3. three quadrangular grids, side by side, were designed and used as basis for model validation;
4. materials properties were applied also considering the composite layout;
5. nominal thicknesses were reduced taking in count the effect of treatments;
6. two-dimentional (shell) elements were employed for spatial discretisation;
7. layered shell method was adopted, including integration points throught the thickness;
8. model validation was successfully performed thanks to a dynamic experiment;
9. modes and frequencies were used as base for this comparison;
10. pre-stress analysis permitted to include the gravity force;
11. validated model was applied for investigating the entire roof behaviour (in two parts);
12. pre-stress analysis permitted to include real constrains, together with the gravity force;
13. the presence of solar cells, laminated on flexible supports, was also considered;
14. natural frequencies were compared with values from literature;
15. the roof was manufactured and installed on the vehicle.

5. Conclusions

The present study describes a redesign intervention of a photovoltaic roof for solar racing vehicles where the indispensable lightness and rigidity must however be balanced with an adequate dynamic behaviour. The dynamic behaviour of the new design solution, based on grid elements instead of perforated plates, was investigated by a modal analysis which took into account all the peculiarities of the system such as: a large three-dimensional profile, a complex double grid conformation, the presence of a sandwich structure, the anisotropy of composite materials, the specific constraint conditions, the presence of additional elements (i.e., the solar cells) acting as rigid reinforcement, the influence of gravity force. The numerical discretization was based on a single layer of shell elements throughout the geometry and integration points throughout the thickness (i.e. 'layered shell' method). Further integration points allowed to better consider the transitions between the layers. Thanks to such methodological enhancements, the model accuracy, evaluated by a comparison between experimental measures and numerical predictions, was very precise (mean error $< 1.5\%$). Later, it was applied to the vehicle design with the scope to investigate the dynamic behaviour of the solar roof under loads and constrains as in reality. The analysis supported the design structure detecting the lowest modal frequencies and comparing them with expected ones with the scope to reduce the risk of resonances. Finally, the roof was manufactured by hand-up process and autoclave technology and installed on the vehicle.

Funding

This research has been carried out within the international collaboration project '*Two Seats for a Solar Car*', an intervention funded by the *Italian Ministry of Foreign Affairs and International Cooperation* (MAECI) with the scope to convert a racing solar car into a solar road vehicle.

CRediT authorship contribution statement

Ana Pavlovic: Software, Validation, Formal analysis, Investigation. **Davide Sintoni:** Software, Investigation, Data curation, Writing - original draft. **Giangiacomo Minak:** Formal analysis, Writing - review & editing, Supervision. **Cristiano Fragassa:** Conceptualization, Methodology, Resources, Data curation, Writing - original draft, Writing - review & editing, Visualization.

Declaration of Competing Interest

The authors declare that they have no known competing financial interests or personal relationships that could have appeared to influence the work reported in this paper.

Acknowledgments

The construction and installation of the composite roof were carried out by members of *Onda Solare Sports Association* at the *MetalTig Srl* workshops (in Castel San Pietro Terme, Italy) with special recognition for their efforts to Mauro Sassatelli and Marco Bertoldi. The authors also thank to Marco Troncossi for providing experimental data for validation.

Appendix A. Supplementary data

Supplementary data to this article can be found online at https://doi.org/10.1016/j.compstruct.2020.112523.

References

[1] Stewart R. Automotive composites offer lighter solutions. Reinf Plast 2010;54 (2):22–8.
[2] Chawla KK, Chawla N. Automotive composites. Wiley Encyclopedia of Composites 2011:1–6.
[3] Li X, Li G, Wang CH, You M. Optimum design of composite sandwich structures subjected to combined torsion and bending loads. Appl Compos Mater 2012;19 (3–4):315–31.
[4] Pitarresi G et al. A comparative evaluation of crashworthy composite sandwich structures. Compos Struct 2007;78(1):34–44.
[5] Heimbs, S.; Strobl, F.; Middendorf, P.; Gardner, S.; Eddington, B.; Key, J. Crash simulation of an F1 racing car front impact structure. In: 7th European LS-DYNA users conference, Salzburg, Austria, 14-15 May 2009.
[6] Njuguna, J. (Ed.). (2016). Lightweight composite structures in transport: design, manufacturing, analysis and performance. Woodhead publishing.
[7] Li Z, Crocker MJ. A review on vibration damping in sandwich composite structures. Int J Acoust Vibration 2005;10(4):159–69.
[8] Khan SU, Li CY, Siddiqui NA, Kim JK. Vibration damping characteristics of carbon fiber-reinforced composites containing multi-walled carbon nanotubes. Compos Sci Technol 2011;71(12):1486–94.
[9] Stobener UWE, Gaul L. Active vibration control of a car body based on experimentally evaluated modal parameters. Mech Syst Signal Pr 2001;15 (1):173–88.
[10] Wamsler, M.; Rose, T. Advanced mode shape identification method for automotive application via modal kinetic energy plots assisted by numerous printed outputs. In: MSC Americas Users' Conference, Universal City, California, 5-8 October 1998; p. 1-17.

[11] Wong J-Y. Effect of vibration on the performance of off-road vehicles. J Terramech 1972;8(4):25–42.
[12] Nahvi H, Fouladi MH, Nor MJM. Evaluation of whole-body vibration and ride comfort in a passenger car. Int J Acoust Vib 2009;14(3):143–9.
[13] Burdzick R, Konieczny L. Application of vibroacoustic methods for monitoring and control of comfort and safety of passenger cars. Solid State Phenom 2014;210:20–5.
[14] Mackerle J. Finite element analyses of sandwich structures: a bibliography (1980–2001). Eng Comput 2002;19(2):206–45.
[15] Rama G, Marinkovic D, Zehn M. High performance 3-node shell element for linear and geometrically nonlinear analysis of composite laminates. Compos B Eng 2018;151:118–26.
[16] González, E.V.; Maimí, P.; Martín-Santos; E., Soto, A.; Cruz, P.; Martín de la Escalera, F.; Sainz de Aja, J.R. Simulating drop-weight impact and compression after impact tests on composite laminates using conventional shell finite elements. International Journal of Solids and Structures 2018, 144-145, 230-247.
[17] Marinković D, Rama G, Zehn M. Abaqus implementation of a corotational piezoelectric 3-node shell element with drilling degree of freedom. Facta Universitatis-Series Mech Eng 2019;17(2):269–83.
[18] Nagaraj, M.H.; Reiner, J.; Vaziri, R.; Carrera, E.; Petrolo, M. Progressive damage analysis of composite structures using higher-order layer-wise elements. Composites Part B: Engineering 2020, 190, art. no. 107921
[19] Valvano S, Carrera E. Multilayered plate elements with node-dependent kinematics for the analysis of composite and sandwich structures. Facta Universitatis- Series Mech Eng 2017;15(1):1–30.
[20] Wang Y, Shi G, Wang X. Displacement and stress analysis of laminated composite plates using an eight-node quasi-conforming solid-shell element. Curved Layered Struct 2017;4(1):8–20.
[21] Leonetti L, Nguyen-Xuan H. A mixed edge-based smoothed solid-shell finite element method (MES-FEM) for laminated shell structures. Compos Struct 2019;208:168–79.
[22] Clough, R. W.; Penzien, J. Dynamics of structures, 3rd ed.; Computers and Structures, Inc.: Berkeley, California, 2003; pp. 16, 33, 171-173.
[23] Bhakte, R. S.; Kulkarni, A. P.; Purandare, P. S. An Overview of Modal Analysis Using Finite Element Method. IJSRD - Int. J. Sci. Res. Dev. 2014, 2.3; pp. 642–645.
[24] Ratnaparkhi SU, Sarnobat SS. Vibration analysis of composite plate. IJMER 2013;3 (1):377–80.
[25] Kumar GAY, Kumar KMS. Free vibration analysis of smart composite beam. Mater Today: Proceedings 2017;4(2):2487–91.
[26] de Mello AV de A et al. Modal analysis of orthotropic composite floors slabs with profiled steel decks. Lat Am J Solids Struct 2008;5(1):47–73.
[27] Zhang, Z., et al. Vibration modelling of composite laminates with delamination damage. In: proceedings of 20th International Congress on Acoustics, Sydney, Australia, 23-27 August 2010; ICA. 2010.
[28] Nikhil MK et al. Modal Analysis of Hybrid Laminated Composite Sandwich Plate. Mater Today: Proceedings 2018;5(5):12453–66.
[29] Petrone G et al. Modal characterisation of recyclable foam sandwich panels. Compos Struct 2014;113:362–8.
[30] Mishra N, Basa B, Sarangi SK. Free vibration Analysis of Sandwich Plates with cutout. IOP Conf Ser: Mater Sci Eng 2016;149:012149.
[31] Schwaar M, Gmur T, Frieden J. Modal numerical–experimental identification method for characterising the elastic and damping properties in sandwich structures with a relatively stiff core. Compos Struct 2012;94(7):2227–36.
[32] Meunier M, Shenoi RA. Dynamic analysis of composite sandwich plates with damping modelled using high-order shear deformation theory. Compos Struct 2001;54(2-3):243–54.
[33] Assarar M, El Mahi A, Berthelot J-M. Damping analysis of sandwich composite materials. J Compos Mater 2009;43(13):1461–85.
[34] Araujo AL et al. Damping optimization of viscoelastic laminated sandwich composite structures. Struct Multidiscip Optim 2009;39(6):569.
[35] Santos FM, Temarel P, Soares CG. Modal analysis of a fast patrol boat made of composite material. Ocean Eng 2009;36(2):179–92.
[36] Song F, Ni Y, Tan Z. Optimization design, modeling and dynamic analysis for composite wind turbine blade. Procedia Eng 2011;16:369–75.
[37] Tomar, A.; Singh, D. Modelling and Analysis of a Chassis Frame by Using Carbon Fiber and E-Glass Epoxy as Composite Material: A Comparative Study. IRJET 2016, 3.04: 2395-0072.
[38] Botkin ME. Modelling and optimal design of a carbon fibre reinforced composite automotive roof. Eng Comput 2000;16(1):16–23.
[39] Lee J et al. Design of roof panel with required bending stiffness using CFRP laminates. Int J Pr Eng Man 2016;17(4):479–85.
[40] Cavazzuti, M., et al. Structural optimization of automotive chassis: theory, set up, design. In: Problemes inverses, Controle et Optimisation de Formes, Paris, France, 2-4 April 2012.
[41] Ermolaeva NS, Castro MBG, Kandachar PV. Materials selection for an automotive structure by integrating structural optimization with environmental impact assessment. Mater Design 2004;25(8):689–98.
[42] Dinesh D, Raju FA. Optimum design and analysis of a composite drive shaft for an automobile by using genetic algorithm and ANSYS. Int J Eng Res Appl 2012;2 (4):1874–80.
[43] Chandru BT, Suresh PM. Finite element and experimental modal analysis of car roof with and without damper. Mater Today: Proceedings 2017;4(10):11237–44.
[44] Huybrechts SM, Hahn SE, Meink TE. Grid stiffened structures: a survey of fabrication, analysis and design methods. Proceedings of the 12th international conference on composite materials (ICCM/12), 1999.
[45] Baker, D., et al. Optimal design and damage tolerance verification of an isogrid structure for helicopter application. In: 44th AIAA/ASME/ASCE/AHS/ASC Structures, Structural Dynamics, and Materials Conference, Norfolk, Virginia, 7-10 April 2003.
[46] Ghadi N et al. Design and FE analysis of composite grid structure for skin stiffening application. IRJET 2017;4(8):792–802.
[47] Huybrechts S, Tsai SW. Analysis and behaviour of grid structures. Compos Sci Technol 1996;56(9):1001–15.
[48] Jadhav P, Mantena PR. Parametric optimization of grid-stiffened composite panels for maximizing their performance under transverse loading. Compos Struct 2007;77(3):353–63.
[49] Wodesenbet E, Kidane S, Pang S. Optimization for buckling loads of grid stiffened composite panels. Compos Struct 2003;60(2):159–69.
[50] Chen H, Tsai SW. Analysis and optimum design of composite grid structures. J Compos Mater 1996;30(4):503–34.
[51] Minak G, Brugo T, Fragassa C, Pavlovic A, Zavatta N, De Camargo F. Structural design and manufacturing of a cruiser class solar vehicle. J Visual Experim 2019;143:e58525.
[52] Pavlovic A, Sintoni D, Fragassa C, Minak G. Multi-objective design optimization of the reinforced composite roof in a solar vehicle. Appl Sci 2020;10:2665. https://doi.org/10.3390/app10082665.
[53] Pastor M, Binda M, Harcarik T. Modal assurance criterion. Procedia Eng 2012;48:543–8.
[54] Banerjee, B.; Chen, J.; Das, R.; Kathirgamanathan, A. Comparison of ANSYS elements SHELL181 and SOLSH190. Technical Report · July 2011.
[55] Wagih, A.M.; Hegaze, M.M.; Kamel, M.A. FE modeling of Satellite's Honeycomb Sandwich Panels Using Shell Approach and Solid Approach. AIAA SPACE and Astronautics Forum and Exposition. 12 - 14 Sep 2017, Orlando, FL.
[56] Bogenfeld R, Kreikemeier J, Wille T. Review and benchmark study on the analysis of low-velocity impact on composite laminates. Eng Fail Anal 2018;86:72–99.
[57] Rajbhandari, S.P.; Scott, M.L.; Thomson R.S.; Hachenberg. D. An approach to modelling and predicting impact damage in composite structures. In Proceedings of the 23rd International Congress of Aeronautical Sciences, Toronto, Canada, September 2002 (pp. 8-13).
[58] ISO 7626-2:2015. Mechanical vibration and shock — Experimental determination of mechanical mobility — Part 2: Measurements using single-point translation excitation with an attached vibration exciter
[59] ISO 7626-5:2019. Mechanical vibration and shock — Experimental determination of mechanical mobility — Part 5: Measurements using impact excitation with an exciter which is not attached to the structure
[60] Avitabile P. Modal space - in our own little world. Exp Tech 2014;38:3–5.
[61] Bedri, R.; Al-Nais, M. O. Prestressed modal analysis using finite element package ANSYS. In: International Conference on Numerical Analysis and Its Applications, Berlin, Heidelberg, 2004; Springer; pp. 171-178.
[62] Agrawal MS, Razik Md. Finite element analysis of truck chassis frame. IRJET 2015;2(3):1949.
[63] Gawande RS, Khan SN. Modal Analysis of Gait Frequency Structure on ANSYS 15.0 based on FEA. IJERT 2016;5(12):376–9.
[64] Liang Z, Hua-Min Q. Mechanical research and development of monocrystalline silicon neutron beam window for CSNS. Chin Phys C 2015;39(9):096001.
[65] Kim, J; Cho D. I. D.; Muller R. S. Why is (111) Silicon a better mechanical material for MEMS?. In: Transducers' 01 Eurosensors XV, Munich, Germany, 10-14 June 2001; Springer: Berlin, Heidelberg, Germany, 2001; p. 662-665.
[66] Matweb, Available online: https://www.matweb.com/search/DataSheet.aspx?MatGUID=b3345507e81642dd8a84bc742670cb74 (accessed on 16 April 2020).
[67] Norli MHM et al. Effect of endcap type in beltline outer using finite element analysis. IOP Conf Ser: Mater Sci Eng 2019;469:012021.
[68] MakeItFrom.com, Available online: https://www.makeitfrom.com/material-properties/Ethylene-Tetrafluoroethylene-ETFE (accessed on 13 April 2020)
[69] Fabrix 360, Available online: https://www.fabrix360.com/what-is-etfe (accessed on 13 April 2020)
[70] Awaja F, Pavel D. Recycling of PET. Eur Polym J 2005;41(7):1453–77.
[71] Goodfellow, Available online: http://www.goodfellow.com/A/Polyethylene-terephthalate.html (accessed on 13 April 2020)
[72] MatWeb, Available online: http://www.matweb.com/search/DataSheet.aspx?MatGUID=a696bdcdff6f41dd98f8eec3599eaa20 (accessed on 13 April 2020)
[73] Polymerdatabase.com, Available online: https://polymerdatabase.com/Commercial%20Polymers/PET.html (accessed on 13 April 2020)
[74] Hooper JM, Marco J. Characterising the in-vehicle vibration inputs to the high voltage battery of an electric vehicle. J Power Sources 2014;245:510–9.
[75] Tuononen AJ, Lajunen A. Modal analysis of different drivetrain configurations in electric vehicles. J Vib Control 2018;24(1):126–36.
[76] Beards, C. Engineering vibration analysis with application to control systems 1995. Elsevier.